

A Bayesian hierarchical approach for spatial analysis of climate model bias in multi-model ensembles

Maeregu Woldeyes Arisido · Carlo Gaetan · Davide Zanchettin · Angelo Rubino

Received: date / Accepted: date

Abstract Coupled atmosphere-ocean general circulation models are key tools to investigate climate dynamics and the climatic response to external forcings, to predict climate evolution and to generate future climate projections. Current general circulation models are, however, undisputedly affected by substantial systematic errors in their outputs compared to observations. The assessment of these so-called biases, both individually and collectively, is crucial for the models' evaluation prior to their predictive use. We present a Bayesian hierarchical model for a unified assessment of spatially referenced climate model biases in a multi-model framework. A key feature of our approach is that the model quantifies an overall common bias that is obtained by synthesizing bias across the different climate models in the ensemble, further determining the contribution of each model to the overall bias. Moreover, we determine model-specific individual bias components by characterizing them as non-stationary spatial fields. The approach is illustrated based on the case of near-surface air temperature bias in the tropical Atlantic and bordering regions from a multi-model ensemble of historical simulations from the fifth phase of the Coupled Model Intercomparison Project. The results demonstrate the improved quantification of the bias and interpretative advantages allowed by the posterior distributions derived from the proposed Bayesian hierarchical framework, whose generality favors its broader application within climate model assessment.

Keywords Bayesian hierarchical method · Climate biases · Climate model uncertainty · Gaussian kernels · Posterior distribution · spatial model.

1 Introduction

Coupled atmosphere-ocean general circulation models (GCMs) use mathematical approximations of the laws of fluid dynamics, thermodynamics and chemistry to simulate the mass and energy transfers and the radiative exchanges within and across the global climate system (Flato et al. 2013). Climate simulations performed with such models provide quantitative estimates of geophysical quantities such as temperature and precipitation, which are used for both investigation of climate dynamics and to produce historical and paleoclimate simulations as well as projections of future climate, where climate changes by virtue of natural as well as anthropogenic forcings can be assessed (e.g., Tebaldi et al. 2005; Flato et al. 2013).

Despite the continuing improvement of climate models, simulations performed with the current generation of GCMs involve substantial uncertainties. The use of so-called multi-model ensembles is a common practice in contemporary climate science, as they allow to overcome the peculiarities of individual simulations, like those linked to the chosen initial conditions and applied external forcing, and the deficiencies of individual models, by combining the information into a multi-model consensus (Lambert and Boer 2001; Neuman 2003; Tebaldi et al. 2005; Sain and Furrer 2010; Kang et al. 2012). The Coupled Model Intercomparison Project phase 5 (CMIP5, Taylor et al. 2012) provides the largest collection of multi-model experiments with state-of-the-art GCMs. It demonstrated that current climate simulations are affected by large systematic errors of the mean state and variability, or biases, i.e., discrepancies between observed and sim-

M.W. Arisido (✉)
E-mail: maeregu.arisido@unive.it
Tel.: +393665067068

M. W. Arisido · C. Gaetan · D. Zanchettin · A. Rubino
Department of Environmental Sciences, Informatics and Statistics, Ca' Foscari University of Venice, Via Torino 155, 30172 Venice, Italy.

ulated characteristics over extensive regions (Wang et al. 2014). These biases are largely attributed to the limited understanding of many of the interactions and feedbacks in the climate system (Jun et al. 2008), inadequate representation of well known processes in climate models and, to some extent, the unpredictability of the climate system itself (Keller 2009; Leith and Chandler 2010). One of the most severe biases shared by different models is the warm sea-surface temperature bias in the southeastern tropical Atlantic (Flato et al. 2013). Multiple causes have been identified at its origin, in different models, including local factors, such as the along-shore windstress and surface heat fluxes (e.g., Wahl et al. 2015; Milinski et al. 2016), and larger-scale or even remote phenomena, such as the propagation into the southeastern tropical Atlantic of downwelling anomalies generated at the equator (e.g. Toniazzo and Woolnough 2014).

In this paper we focus on assessing climate model biases in multi-model ensembles. It is debated how the information brought by the different models in a multi-model ensemble should be optimally combined to generate consensus: current climate models have been developed by sharing model components (Jun et al. 2008; Flato et al. 2013), and so they are not always independent from each other (e.g., Knutti 2010). The consequent weighting models based on arguments such as model independence can substantially affect the estimation of multi-model consensus and associated uncertainty (Knutti 2010; Flato et al. 2013).

We present a spatial analysis based on the Bayesian hierarchical model that provides a unified assessment of the biases within a multi-model context. Specifically, the proposed probabilistic approach allows to estimate the overall bias component, i.e., the component of the bias which is the same for all models, and the individual model biases, i.e., the components of the bias that are specific of each model, further characterizing each model's contribution to the overall bias and related uncertainty. We describe the different bias components as non-stationary spatial fields.

Our approach represents therefore a step forward compared to previous assessments of climate model biases based on Bayesian hierarchical modeling, which dealt with spatially aggregated geophysical data (e.g., Christensen et al. 2008; Buser et al. 2009) or grid-points individually (e.g., Boberg and Christensen 2012).

We illustrate the method by using observational reference data and an ensemble of six historical full-forcing climate simulations contributing to CMIP5. We focus on an application involving spatially referenced near-surface air temperature averaged over the years 1950-2005, and covering the tropical Atlantic Ocean and bordering regions.

In the following section, we describe the data and present our definition of climate model bias. Section 3 discusses the Bayesian hierarchical method tailored for a unified assessment of climate model biases in a multi-model framework,

while section 4 illustrates the results. We provide a concluding discussion in section 5.

2 Data and climate model biases

The dataset comprises observational reference and climate model outputs. Although the latter are obtained from deterministic numerical models, it is a common practice to consider the model output as 'data', which may not represent the traditional statistical definition of data.

2.1 Observations and GCM output

We use monthly-mean data obtained from the NCEP reanalysis (Kalnay et al. 1996; Kistler et al. 2001) as our observational reference data. Reanalysis data are the output of a state-of-the-art analysis/forecast system with data assimilation using past data from 1948 to the present. The data were provided by the NOAA/OAR/ESRL PSD, Boulder, Colorado, USA. Reanalysis data are therefore not direct observations, yet they facilitate the purposes of this study by providing gridded records of absolute temperatures. This is an advantage compared to other observational products that provide anomalies as main gridded output, such as the temperature series produced by the Climatic Research Unit of the University of East Anglia (Brohan et al. 2006). Our climate model outputs are based on monthly-mean data from an ensemble of six historical full-forcing climate simulations contributing to CMIP5. An overview of the models' characteristics is provided in Table 1, see Zanchettin et al. (2015) for more details on the models and the simulations. The analysis is for the period 1950-2005 CE for which we derive climatologies of annual-mean values starting from the monthly-mean time series of both observations and simulations over the tropical Atlantic region. Geographically the tropical Atlantic is defined here as the region covering the latitude range 35°S to 15°N and the longitude range 40°W to 20°E.

2.2 Climate model biases

Climate model bias is determined by comparing output data against observations. We let $Y(s)$ represent the temperature observations and $X_j(s)$ denote the temperature simulated by the climate model j at the spatial location $s \in D$ for the domain $D \subset \mathbb{R}^2$. One crucial aspect of the complexity inherent in the assessment of climate model biases is the spatial misalignment between observations and model output. The fact that model output and observations are provided on different grids may hinder statistical analysis of the bias at the grid-point level. To tackle this issue, we interpolated the output

Table 1 The six general circulation models (GCMs) utilized for this study. BCC stands for BCC-CSM1-1 and GISS: GISS-E2-R, IPSL: IPSL-CM5A-LR, MPI: MPI-ESM-P and MIROC: MIROC-ESM. The ensemble has also been used by Zanchettin et al. (2015).

GCMs	Atmospheric resolution	Research center
CCSM4	1.25°N × 0.94°E	National Center for Atmospheric Research (USA)
BCC	2.81°N × 2.75°E	Beijing Climate Center (China)
IPSL	3.75°N × 1.90°E	Institute Pierre Simon Laplace (France)
MPI	1.88°N × 1.90°E	Max Planck Institute for Meteorology (Germany)
GISS	2.50°N × 2.00°E	NASA/Goddard Institute for Space Studies (USA)
MIROC	2.81°N × 2.75°E	Center for Climate System Research (Japan)

159 data on the regular observational grid to ensure that $Y(s)$
 160 and $X_j(s)$ are aligned on the same grid (see, e.g., Jun et al.
 161 2008; Banerjee et al. 2014). Empirical climate model biases
 162 are then calculated as

$$B_j(s) = Y(s) - X_j(s), \quad j = 1, \dots, 6 \quad (1)$$

163 where $B_j(s)$ denotes the bias of climate model j relative
 164 to the observation at spatial location s . For n sites in D ,
 165 we observe the biases, namely $\{B_j(s_i), \dots, B_j(s_n)\}$. Figure
 166 1 summarizes the bias fields of near-surface air temperature
 167 in the tropical Atlantic region from the six climate models.
 168 Clearly, the different GCMs produce similar spatial features
 169 of the bias. For instance, all models produce a warm bias
 170 over the Angola-Benguela front region. We also note distinct
 171 features for each model bias. For instance, the above
 172 mentioned warm bias in the Angola-Benguela front region
 173 has different severity in the different models, with peak
 174 values ranging from 3 kelvin in CCSM4 to 5 kelvin on MIROC,
 175 and can extend either to the north, like in CCSM4, GISS and
 176 IPSL, or to the south, like in MIROC and BCC. Also, the
 177 south Atlantic mid-latitudes can feature either an extensive
 178 negative bias, like in CCSM4, BCC and MIROC, or an ex-
 179 tensive positive bias, like in GISS and IPSL. The remainder
 180 of this paper devotes to quantifying the shared bias and the
 181 individual components and associated uncertainties across
 182 the different climate models.

183 3 Bayesian hierarchical approach for climate model 184 biases

185 Our aim is to obtain a statistical representation of climate
 186 model biases in a multi-model ensemble that separates an
 187 overall common bias from the individual components. We
 188 present a Bayesian hierarchical model formulated based on
 189 three levels: *data*, *process*, and *parameters* (Berliner 2003).
 190 The data model captures the information given in the form of
 191 empirically measured biases, conditional on a hidden spatial
 192 bias process. The process level models the spatial structure
 193 and links the hidden spatial process to a set of parameters.
 194 In the parameter model, prior distributions are specified for

the parameters. The three levels are specified in terms of
 probability distributions in a hierarchical structure

$$\begin{cases} [\text{data}|\text{process}] : \text{Data model} \\ [\text{process}|\text{parameters}] : \text{Process model} \\ [\text{parameters}] : \text{Parameter model,} \end{cases}$$

where $[A|B]$ denotes a conditional probability distribution of
 A given B and $[A]$ denotes the probability density of A .

3.1 Data model

We assume that the empirical bias $B_j(s)$ can be decomposed
 into two components: a spatial component $M_j(s)$ and a noise
 component $\varepsilon_j(s)$, namely

$$B_j(s) = M_j(s) + \varepsilon_j(s), \quad j = 1 \dots, 6 \quad (2)$$

Here $\{\varepsilon_j(s)\}$ is a Gaussian white noise with zero mean and
 variance $\sigma_{\varepsilon,j}^2$, independent from $\{\varepsilon_k(s)\}$, for $k \neq j$. Addi-
 tionally, the noise component $\{\varepsilon_j(s)\}$ is assumed indepen-
 dent from $\{M_j(s)\}$. Thus, conditionally on the spatial pro-
 cess $\{M_j(s)\}$, the observed bias $B_j(s)$ has a Gaussian dis-
 tribution with mean $M_j(s)$, and variance $\sigma_{\varepsilon,j}^2$ that represents
 the data model level.

3.2 Process model

GCM ensemble members feature biases which may origi-
 nate from different factors including parameterizations, dis-
 cretization to solve the numerical equations, resolution level
 and imposed boundary conditions. The spatial process $\{M(s)\}$,
 with $M(s) = (M_1(s), \dots, M_6(s))'$ is multivariate, and can be
 modeled in different ways (Gelfand et al. 2010). Here we
 assume that the climate bias can be additively decomposed
 into two components

$$M_j(s) = \mu(s) + \eta_j(s), \quad j = 1, \dots, 6, \quad (3)$$

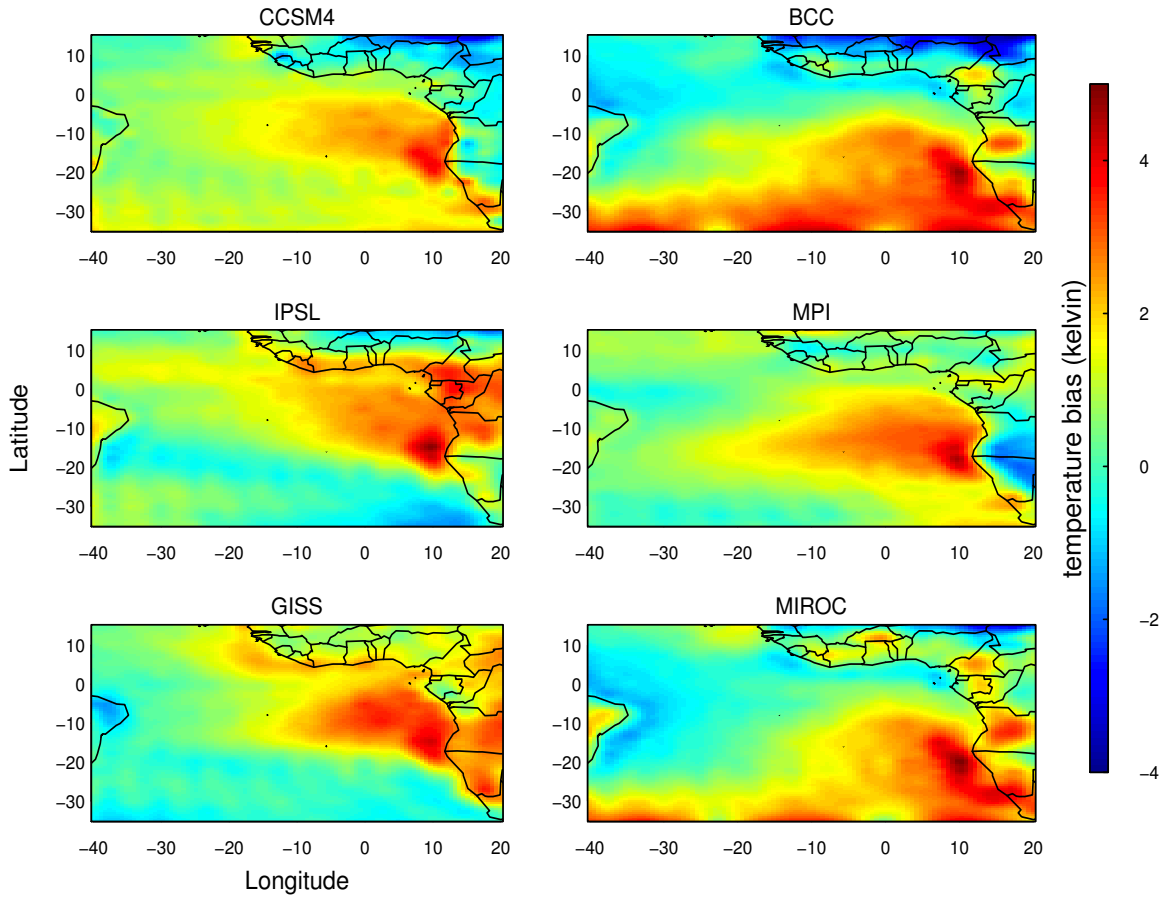


Fig. 1 Empirical bias for simulated near-surface air temperature for each of the six GCMs in the ensemble relative to the observed temperature over the tropical Atlantic region.

219 where $\mu(s)$ is the overall common bias capturing shared
 220 large-scale features for all climate models, while $\eta_j(s)$
 221 describes the j th model-specific features. Based on this inter-
 222 pretation, specification (3) can be viewed as a version of a
 223 random effect model (see Furrer et al. 2007; Kaufman and
 224 Sain 2010; Kang et al. 2012, for examples of applications
 225 in climatology). To model the two spatial components $\mu(s)$
 226 and $\eta_j(s)$, we adopt an approach based on kernel basis func-
 227 tions (see, e.g., Higdon 1998) and we suppose that

$$\mu(s) = \mathbf{w}(s)' \alpha_k \quad \eta_j(s) = \mathbf{w}^*(s)' \mathbf{v}_j, \quad (4)$$

228 where $\mathbf{w}(s) = \{w_1(s), \dots, w_p(s)\}'$, $\mathbf{w}^*(s) = \{w_1^*(s), \dots, w_{p^*}^*(s)\}'$
 229 are vectors of Gaussian kernels and $\alpha = (\alpha_1, \dots, \alpha_p)'$ and
 230 $\mathbf{v}_j = \{v_{j,1}, \dots, v_{j,p^*}\}'$ are vectors of parameters. The shape
 231 and number of kernels associated to $\mathbf{w}(s)$ and $\mathbf{w}^*(s)$ are dif-
 232 ferent. Since the individual components $\{\eta_j(s) : j = 1, \dots, 6\}$
 233 aim to capture local-scale features, a larger number p^* of
 234 kernels with a narrower spatial bandwidth are expected to be
 235 required with respect to that necessary to describe the

236 overall common bias $\mu(s)$, i.e., $p < p^*$. However, the num-
 237 ber of kernels p and p^* will be much less than the num-
 238 ber of data points n . The choice of the kernels and their
 239 shapes is further discussed in section 3.4. The parameters
 240 α and $\{\mathbf{v}_j, j = 1, \dots, 6\}$ are considered as random. More
 241 precisely α is multivariate Gaussian $\alpha \sim \text{Gau}(\mathbf{0}, \mathbf{G})$, where
 242 \mathbf{G} is the $p \times p$ covariance matrix, and $\{\mathbf{v}_j, j = 1, \dots, 6\}$
 243 are mutually independent zero mean Gaussian processes,
 244 $\mathbf{v}_j \sim \text{Gau}(\mathbf{0}, \tau_j^2 I_{p^*})$, where $\tau_j^2 I_{p^*}$ is the covariance matrix
 245 and I_{p^*} is the $p^* \times p^*$ identity matrix. With this setup $\eta_j(s)$
 246 is a Gaussian random variable with zero mean and variance
 247 $\text{var}(\eta_j(s)) = \tau_j^2 \mathbf{w}^*(s)' \mathbf{w}^*(s)$. Thus the parameters τ_j^2 mea-
 248 sure how each climate model bias varies about the over-
 249 all common bias. More specifically, different values of τ_j^2
 250 across the various models indicate different levels of de-
 251 parture from the common bias. Alternatively, similar values
 252 of τ_j^2 for different models indicate that they vary similarly
 253 about the overall common bias, suggesting that the contribu-
 254 tion of each climate model in estimating the overall common
 255 bias is similar. Under these hypotheses we have constructed

a non-stationary spatial process for $M_j(s)$ with covariance function

$$\begin{aligned} \text{cov}(M_j(s), M_j(s')) &= \sum_{m=1}^p \sum_{k=1}^p G_{mk} w_m(s) w_k(s') + \\ &\tau_j^2 \sum_{m=1}^{p^*} \sum_{k=1}^{p^*} w_m^*(s) w_k^*(s') \end{aligned} \quad (5)$$

where $G_{mk} = \text{cov}(\alpha_m, \alpha_k)$ is the m, k entry of the covariance matrix \mathbf{G} , and cross-covariance function

$$\text{cov}(M_j(s), M_l(s')) = \sum_{m=1}^p \sum_{k=1}^p G_{mk} w_m(s) w_k(s'), \quad j \neq l. \quad (6)$$

3.3 Parameter model

In the parameter level, we specify prior probability distributions for the model parameters $\{(\sigma_{\varepsilon,1}^2, \tau_1^2), \dots, (\sigma_{\varepsilon,6}^2, \tau_6^2), \mathbf{G}\}$. Prior distributions for these parameters are generally taken to be non-informative. For $\sigma_{\varepsilon,j}^2$, we assign a proper uniform prior on the standard deviation scale $\sigma_{\varepsilon,j} \sim \text{Unif}(a, b)$ for each j independently. The values of the hyperparameters a and b are chosen so as to obtain an approximately non-informative prior. For $\{\tau_j^2\}$, we use the Half-Cauchy (HC) prior with scale parameter θ . We avoid using the usually implemented inverse-gamma priors, since these priors do not yield a proper posterior if the priors are taken to be non-informative. This was confirmed by our preliminary assessment (not shown) and supported by Gelman (2006) and Polson and Scott (2012). We specify the HC prior as $\tau_j \sim \text{HC}(\theta)$ for each j independently. Large but finite values of θ represent approximately non-informative prior distributions. See the appendix for further details on prior and hyperparameter choices. We also need to specify the prior distribution for the covariance matrix \mathbf{G} . The inverse Wishart (IW) prior has been proposed for covariance matrices like \mathbf{G} , with scale parameter the identity matrix \mathbf{I}_p and $p+1$ degrees of freedom. Although computationally convenient, the IW family is found to be quite constraining as p is the only 'tuning parameter' available to express uncertainty in the elements of \mathbf{G} (Gelman and Hill 2006; Leith and Chandler 2010). We use the modified version of the IW (see, e.g., Gelman and Hill 2006; O'Malley et al. 2008) which is based on the decomposition $\mathbf{G} = \Gamma \mathbf{Q} \Gamma$, where Γ is a diagonal matrix with the scaling elements $\{\omega_k^2\}$ being given non-informative uniform priors over a wide range, and $\mathbf{Q} \sim \text{IW}(p+1, \mathbf{I}_p)$. We then determine \mathbf{G} by computing its diagonal and off-diagonal elements, $G_{kk} = \omega_k^2 Q_k$ and $G_{kl} = \omega_k^2 \omega_l^2 Q_{kl}$ for $k, l = 1, \dots, p$.

3.4 The choice of the kernels

Several types of kernel functions have been used in the literature, including Gaussian kernels (Stroud et al. 2001) and bisquare functions (Kang et al. 2012). In this paper we have considered a Gaussian kernel specified as

$$w_k(s) \propto \exp\{-(s - c_k)' \Sigma^{-1} (s - c_k) / 2\}, \quad (7)$$

where c_k denotes the center of the kernel and Σ determines the shape. The number of kernels, p or p^* , their locations and shapes must be chosen. These choices are often based on the presence of prior information such as smoothness and spatial dependence related to the spatial process (Stroud et al. 2001). If we choose spherically shaped kernels, i.e., $\Sigma = \kappa \mathbf{I}_2$ on R^2 and $\kappa > 0$, and the centers belong to a regular grid over an unbounded domain, (5) approximates a covariance function of a stationary isotropic process when the number of kernels is very large. Alternatively, a geometrically anisotropic process may be obtained if we choose non-spherical Gaussian kernels. One way to investigate whether the spatial biases are direction-dependent or not is to perform variogram analyses of the biases for different directions (Cressie 1993). A variogram provides a descriptive statistic of the spatial continuity of a data set. Empirical variograms are calculated by averaging the semi-variances over all pairs of available observations, with a specified separation distance and direction. Figure 2 illustrates the empirical variograms of the six GCM biases for the directions: $0^\circ, 45^\circ, 90^\circ, 135^\circ$ (i.e. North, Northeast, East and Southeast direction, respectively). Observing the plots of the variograms within each panel does not reveal strong anisotropy in the four directions at small distances since the patterns are not largely different. This suggests that we can safely choose a spherical kernel.

Figure 3 shows the two different sets of centers which are used for our main analysis. Panel (a) shows $p = 36$ equally-spaced Gaussian kernels with scale $\Sigma = 0.6 \mathbf{I}_2$ on R^2 , which are used to model $\mu(s)$. Panel (b) shows $p^* = 45$ unequally-spaced Gaussian weighting kernels with the smaller scale $\Sigma = 0.4 \mathbf{I}_2$, which are used to model $\eta_j(s)$. In section 4 we present a sensitivity analysis for the kernel choice, and discuss the advantages and drawbacks of different choices.

3.5 MCMC simulations

Parameter estimation and inference is based on a Bayesian context by sampling from the posterior probability distribution, which is generalized as

$$\begin{aligned} [\text{process}, \text{parameters} | \text{data}] \propto & [\text{data} | \text{process}] \times \\ & [\text{process} | \text{parameters}] [\text{parameters}]. \end{aligned}$$

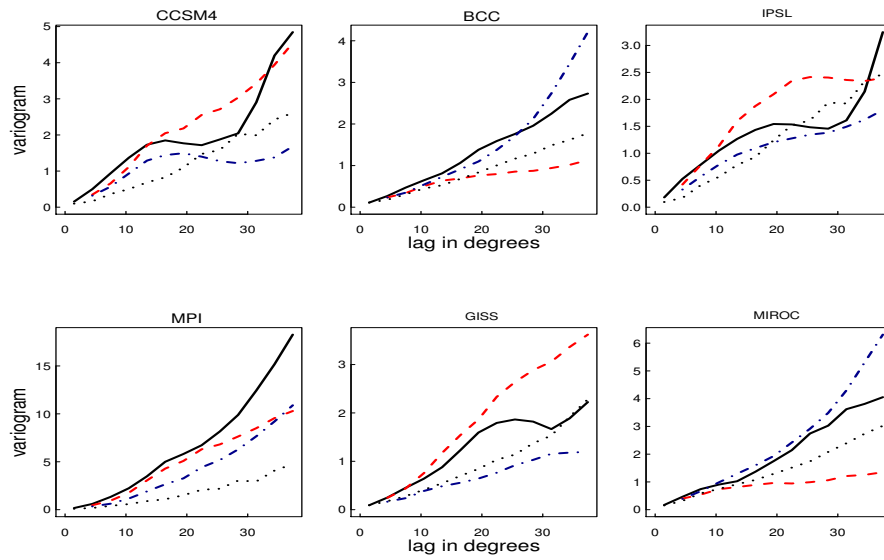


Fig. 2 Empirical variograms of the six GCM biases of the tropical Atlantic region for four different directions (black solid 0° , red dashed 45° , gray dotted 90° , blue dash-dotted 135°). The variograms were analyzed using the robust estimator as given by Cressie (1993).

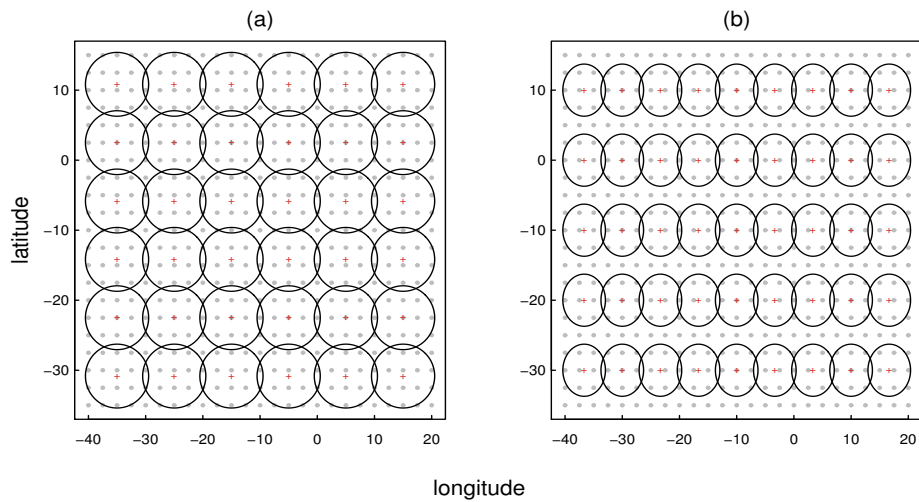


Fig. 3 (a) The 36 equally-spaced Gaussian kernels that are used to model $\mu(s)$; (b) The 45 unequally-spaced Gaussian kernels that are used to model $\eta_j(s)$. Gray color bullets indicate data locations and red color crosses indicate centers of the kernels.

The posterior distributions corresponding to $\mu(s)$ and $\eta_j(s)$ cannot be obtained in closed form, so we use the Markov Chain Monte Carlo (MCMC) method (Gilks et al. 1996) with Gibbs sampler that adopt full conditional distributions. For the MCMC simulations we used three chains, each with overdispersed starting values. We performed 50000 simulations discarding the first 20000 as burn-in. The remaining samples were thinned at every tenth step to reduce autocorrelations of successive samples, from which the remaining 3000 draws were used for posterior analyses. We performed the computations by using the OpenBUGS (version 3.2.3) statistical software package. The computation time depends mainly on the size of the kernel vectors. For example, if we use 36 Gaussian kernels to describe both $\mu(s)$ and $\eta_j(s)$, the computations take about 10 hours on a 64-bit OS X 10.10.5 Intel Core i5 1.6 GHz. Posterior convergence was assessed by inspecting the simulation history of a sample of parameters using graphical tools and the Gelman-Rubin formal convergence diagnostic (Cowles and Carlin 1996). We then summarized the MCMC draws in terms of mean, median and standard deviation to make posterior inference about the unknowns.

4 Results

Figure 4 summarizes the posterior results with respect to the overall climate model bias $\mu(s)$. Panel (a) presents the posterior mean of the overall common bias $\mu(s)$ using the 36 Gaussian kernels that are shown in Figure 3(a). The posterior standard deviations of $\mu(s)$ is shown in Figure 4(b). To better understand $\mu(s)$, Figure 4(c) shows the empirical bias which is estimated as a simple average of the biases from the six GCMs with the underlying assumption that all GCMs have equal weight in synthesizing the overall common bias. The posterior mean of the overall bias and its associated empirical estimate agree well on the general features of the bias over the whole tropical Atlantic region. Common features include the warm error over the southeastern tropical Atlantic, which reaches peak values exceeding 4 kelvin over the Angola-Benguela front region and extends westward as far as 10°W . Both estimates capture a cold error of similar severity over the western tropical Atlantic ocean, along the South American coast. Shared features over landmasses include the cold error over the subsaharan region and warm errors over major near-coastal mountainous African regions, such as the Cameroon line and the Namib desert. Compared to the empirical estimate, the posterior mean of the overall bias intensifies the cold errors over the western Kalahari and over the Congo river, while reducing the cold error over the subsaharan region. The posterior standard deviations of the overall common bias (Figure 4(b)) suggest that its estimate is largely uncertain in the southeastern tropical Atlantic, over the Angola-Benguela front region, where the

largest bias is observed. Uncertainty in the common bias estimate is large also along the African coast, possibly reflective of the diversity in the representation across models of coastal topography and/or freshwater discharge processes. The bias estimate is, conversely, more certain in regions affected by cold errors, such as the subsaharan region and the western tropical Atlantic Ocean.

Overall, the posterior mean estimate of the overall bias has a smoother spatial pattern than the corresponding empirical estimate, which changes more rapidly, in the longitude-latitude space. The similarity of the bias patterns in Figure 3(a) and (c) suggests that the proposed method highlights the same common features of the bias that are reflected in the empirical bias estimate. Nonetheless, the Bayesian approach allows to gain deeper insights about how much each climate model varies around the overall common bias. As pointed out in section 3.2, the variance parameters $\{\tau_j^2 : j = 1, \dots, 6\}$ are useful to assess how each climate model bias varies about the overall common bias. Figure 4(d) depicts the posterior medians of τ_j along with the 25th and 75th percentiles, which show a marked difference across the individual GCMs about the overall common bias. CCSM4 varies the least, whereas IPSL and GISS vary the most about the overall common bias. Thus, in terms of weighting the contributions of each GCMs in synthesizing the overall common bias, CCSM4 is ranked first, whereas IPSL and GISS have smaller weights. One benefit of the Bayesian hierarchical method is that it allows to determine the heterogeneity across the climate models, highlighting the limitations of the equal weight assumption often adopted in the traditional empirical estimate.

We now provide posterior assessments of the individual bias components $\{\eta_j(s) : j = 1, \dots, 6\}$. These individual components measure the departure of each climate model bias from the overall common bias $\mu(s)$. As compared to $\mu(s)$, $\eta_j(s)$ describe model-specific local features. Thus, we use a relatively large number of kernels $p^* = 45$, which are shown in Figure 3(b). Figure 5 shows the posterior means of $\{\eta_j(s) : j = 1, \dots, 6\}$. The values of $\eta_j(s)$ for CCSM4 are overall the smallest among all models in the ensemble, suggesting that the most prominent features of CCSM4 go to the overall common bias. This is consistent with our previous result that CCSM4 varies the least about the overall common bias, see Figure 4(d). Similarly, as expected from Figure 4(d), IPSL shows large departures from the overall common bias, followed by GISS. All models show warm errors over the Angola-Benguela front region in their individual bias components. This counterintuitive result is explained by the different location of the peak warm error across the different models, i.e., all models feature a warm bias in the Angola-Benguela front region captured by $\mu(s)$, but each with model-distinctive intensity and spatial structure, which

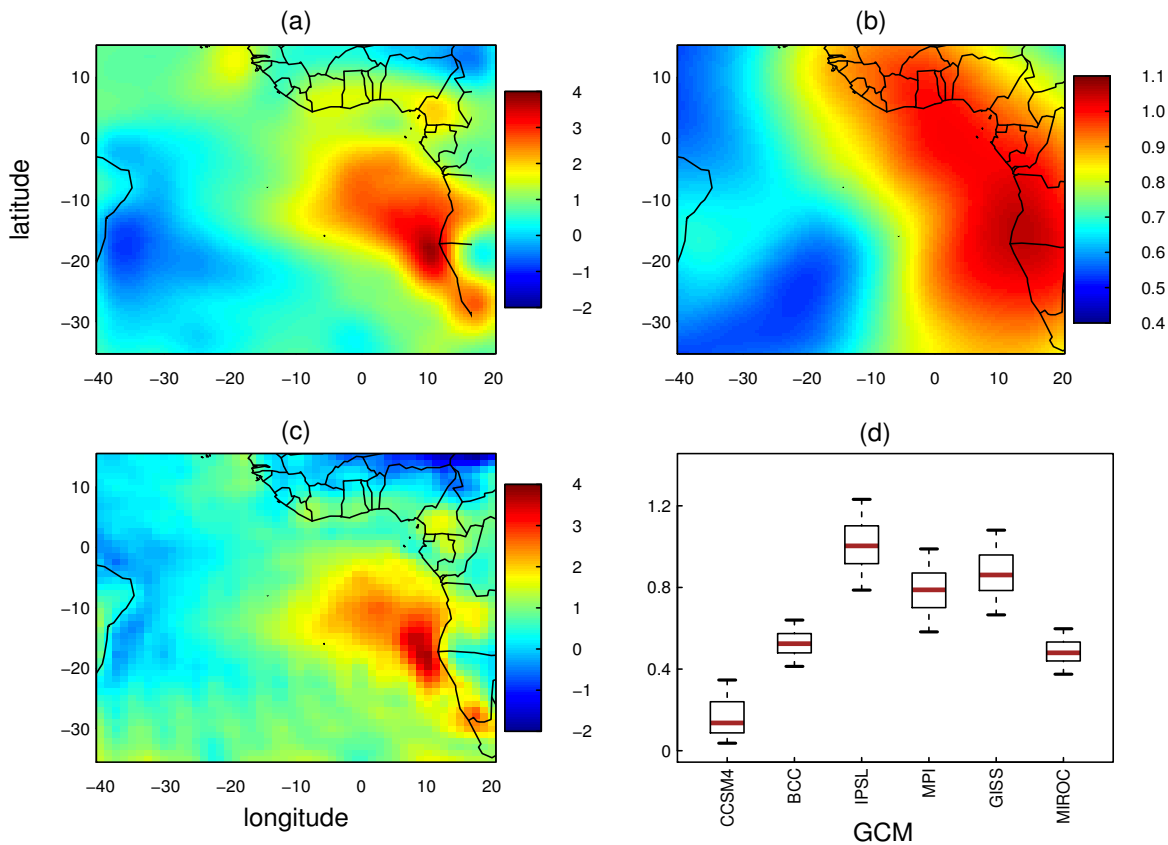


Fig. 4 (a) Posterior mean of the overall common bias $\mu(s)$; (b) associated posterior standard deviation of the overall common bias; (c) empirical estimate of climate model bias, obtained by naively averaging the six climate models assuming the same weight for all of them; (d) Boxplots of the posterior samples of the standard deviation parameters $\{\tau_j : j = 1, \dots, 6\}$ where the bold solid horizontal bars denote the medians, the lower and upper bars of the boxes indicate the 25th and 75th percentiles respectively.

439 are captured by $\eta_j(s)$. The extratropical South Atlantic is
 440 the region where the largest variability in $\eta_j(s)$ value is de-
 441 tected, particularly due to the large values of opposite sign
 442 in GISS and BCC.

443 4.1 Model assessment

444 We now investigate the adequacy of our modeling approach
 445 to the choices of Gaussian weighting kernels and hyperpa-
 446 rameters. In particular, we recall that our model fitting re-
 447 quires specifying (1) the number of weighting kernels, (2)
 448 the scale of the kernels (Σ) and (3) the locations or cen-
 449 ters of the kernels. To assess the robustness of the results
 450 with respect to these choices, we perform a sensitivity anal-
 451 ysis for the overall bias $\mu(s)$ using three different numbers
 452 of kernels, that is $p \in \{15, 28, 48\}$, three different choices
 453 of scale of the kernels, that is $\Sigma \in \{0.1\mathbf{I}_2, 1.2\mathbf{I}_2, 5\mathbf{I}_2\}$ where
 454 \mathbf{I}_2 is the identity matrix on R^2 , and three different sets of
 455 kernel locations. Figure 6 presents the contour plots of the
 456 overall common bias $\mu(s)$ associated to the different choices

of p and Σ . The three panels in the upper row show the con-
 457 tour plots of $\mu(s)$ fixing $\Sigma = 0.5\mathbf{I}_2$ while varying p . A value
 458 of $p = 15$ results in a smooth pattern of $\mu(s)$, which fea-
 459 tures a peak warm bias of 1.5 kelvin in the Angola-Benguela
 460 front region, which is displaced westward compared to the
 461 empirical estimate as well as to Bayesian hierarchical esti-
 462 mates obtained with larger p values. The pattern also misses
 463 many of the topographic characteristics recognizable from
 464 Figure 4. With a larger number of kernels ($p = 48$), the over-
 465 all common bias appears to be more jagged lacking enough
 466 smoothness, while it produces a more detailed spatial pat-
 467 tern. The choice of $p = 28$ (panel b) produces smoothed
 468 contour lines and a warmer bias of about 3 kelvin in the
 469 Angola-Benguela front region, which is closer to the empir-
 470 ical average as well as to the Bayesian estimate. The three
 471 panels in the lower row display the contour plots for the
 472 overall common bias estimated by fixing $p = 15$ while vary-
 473 ing $\Sigma \in \{0.1\mathbf{I}_2, 1.2\mathbf{I}_2, 5\mathbf{I}_2\}$. We use a low value for $p = 15$
 474 in order to amplify the effect of changes in Σ . The choice
 475 of Σ seems to have the opposite impact of the choice of p :
 476

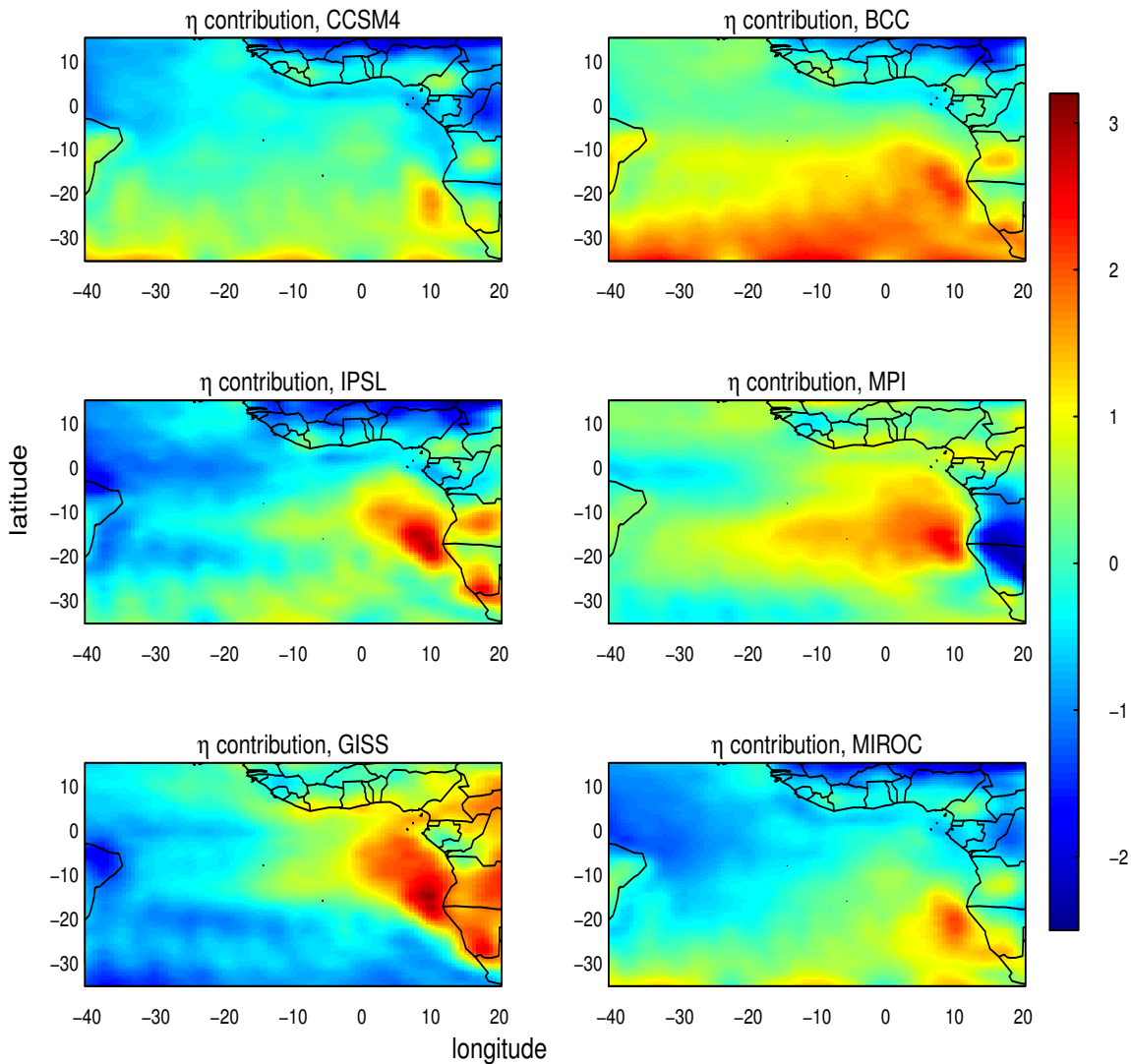


Fig. 5 Posterior means of the individual components $\{\eta_j(s), j = 1, \dots, 6\}$ (in kelvin) associated to the six GCMs in the ensemble.

477 smaller Σ values lead to poorly smoothed $\mu(s)$ (panel d),
 478 while larger Σ strongly smooths $\mu(s)$ (panel f). Overall, the
 479 choice of the kernel parameters, and particularly the number
 480 of kernels p is crucial to capture the inherent spatial bias pro-
 481 cess. In fact, increasing p brings not only increased spatial
 482 details but also noticeable changes in the large scale shape
 483 of the posterior mean of the overall common bias including
 484 the location and magnitude of bias features in key locations.

485 To assess how the choice of kernel locations or centers of
 486 the kernels influences the results, we compare three different
 487 sets of kernels that only differ for the location of the centers
 488 while using the same number of kernels $p = 64$ and scale
 489 matrix $\Sigma = 0.5\mathbf{I}_2$. Figure 7 shows the three sets of kernels,
 490 along with the corresponding surface plots of the posterior
 491 mean of the overall bias $\mu(s)$. The three different sets of ker-
 492 nels are shown in column (a). In the upper row the centers

of the kernels are equally-spaced. The middle and the lower
 493 rows feature two different sets of unequally-spaced kernel
 494 centers. The different kernel locations yield noticeable differ-
 495 ences in the large scale shape of $\mu(s)$ (column b) includ-
 496 ing the location and magnitude of the bias. The most promi-
 497 nent feature is that equally-spaced kernel locations produce
 498 a stronger and more extensive warm bias over the Angola-
 499 Benguela front region compared to unequally-spaced kernel
 500 setups, which is also closer to the bias estimates shown in
 501 Figure 4. The unequally-spaced kernels lead to reduced bias
 502 in both warm and cold bias regions.
 503

We performed a further sensitivity analysis to assess the sen-
 504 sitivity of the results to the choice of the parameter θ of the
 505 Half-Cauchy (HC) prior for τ_1, \dots, τ_6 . While the sensitivity
 506 analysis could be performed for all prior choices, we only
 507 focus on θ as hyperparameters of variance components are
 508

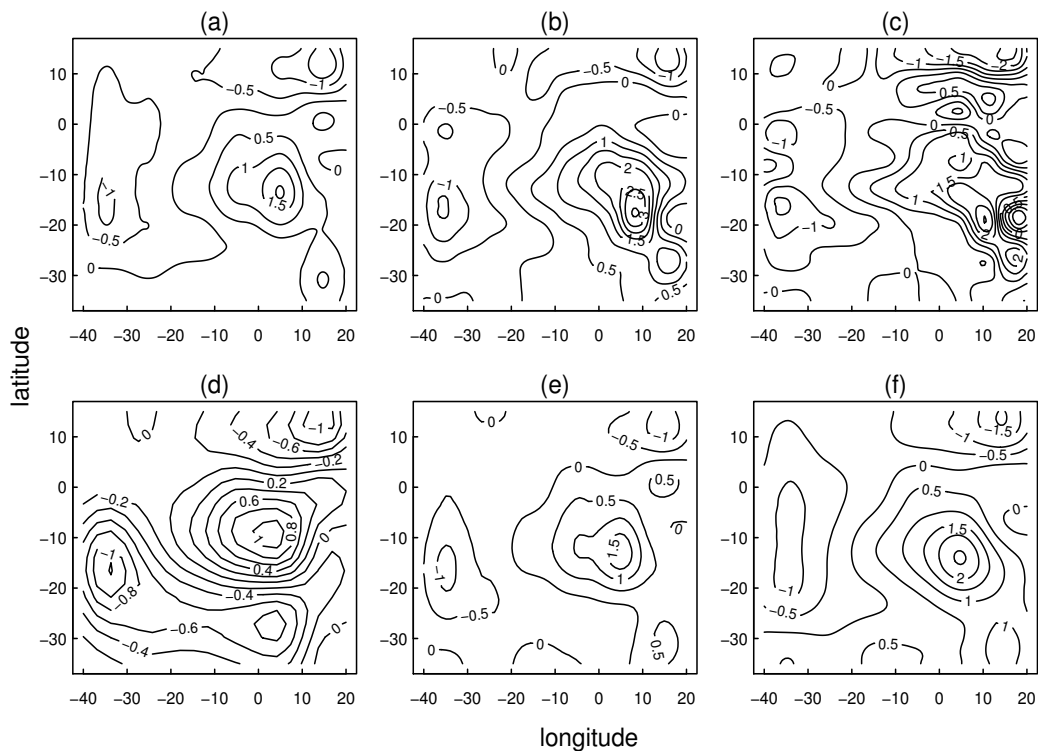


Fig. 6 Assessing the influence of choice of the number p and scale Σ of Gaussian kernels. The upper row shows contour plots of the overall common bias $\mu(s)$ fixing $\Sigma = 0.5\mathbf{I}_2$ while p varies: (a) $p = 15$; (b) $p = 28$; (c) $p = 48$. The lower row shows contour plots of $\mu(s)$ fixing $p = 15$ while Σ varies: (d) $\Sigma = 0.1\mathbf{I}_2$; (e) $\Sigma = 1.2\mathbf{I}_2$; (f) $\Sigma = 5\mathbf{I}_2$.

509 more sensitive than the hyperparameters of other forms such as Gaussian prior for regression coefficients (Gelman 2006).
 510 Figure 8 illustrates the posterior distributions of τ_j for the three choices $\theta \in \{20, 35, 40\}$. The three choices produce
 511 slightly different posterior distributions, but they reflect the same general pattern. The sensitivity to θ differs slightly
 512 across the ensemble members. For instance, CCSM4 provides the smallest variation across all three choices and IPSL
 513 produces the largest variation. Thus, we consider the results to be robust against the specific choice of θ .

519 5 Discussion

520 We have proposed a Bayesian hierarchical method for the probabilistic assessment and quantification of spatially refer-
 521 enced climate model biases in a multi-model ensemble. The approach synthesizes an overall shared bias as a non-
 522 stationary spatial field and quantifies the associated uncertainty. The approach optimizes the way information about
 523 the bias is combined within the ensemble. Specifically, the presented model accounts for the variability of the bias across
 524 the ensemble members, and the contribution of each member to the overall common bias is determined based on the poste-
 525 rior inferences on each model's variability parameter.

528 ensemble members, and the contribution of each member to the overall common bias is determined based on the poste-
 529 rior inferences on each model's variability parameter.
 530

531 Application of the model to the case of tropical Atlantic near-surface air temperature from an ensemble of six histor-
 532 ical simulations contributing to CMIP5 exemplified how the proposed approach allows to gain deeper insights into cli-
 533 mate model bias compared to more traditional assessments: Known common features of the bias in this region are well
 534 captured by our statistical model, such as the warm bias over the Angola-Benguela front region. But, our model further
 535 reveals that the different GCMs unequally contribute to determining this bias, which also results in a variety of model-
 536 specific features of the bias over the same area. The proposed statistical decomposition of each model's bias into a
 537 shared/common and a model-specific component stimulates additional investigation of the underlying physical processes
 538 as well. In our application, for instance, the errors of opposite sign emerging in the model-specific components of
 539 the bias over the near-coastal oceanic waters of equatorial Africa deserve further analysis.
 540
 541
 542
 543
 544
 545
 546
 547
 548

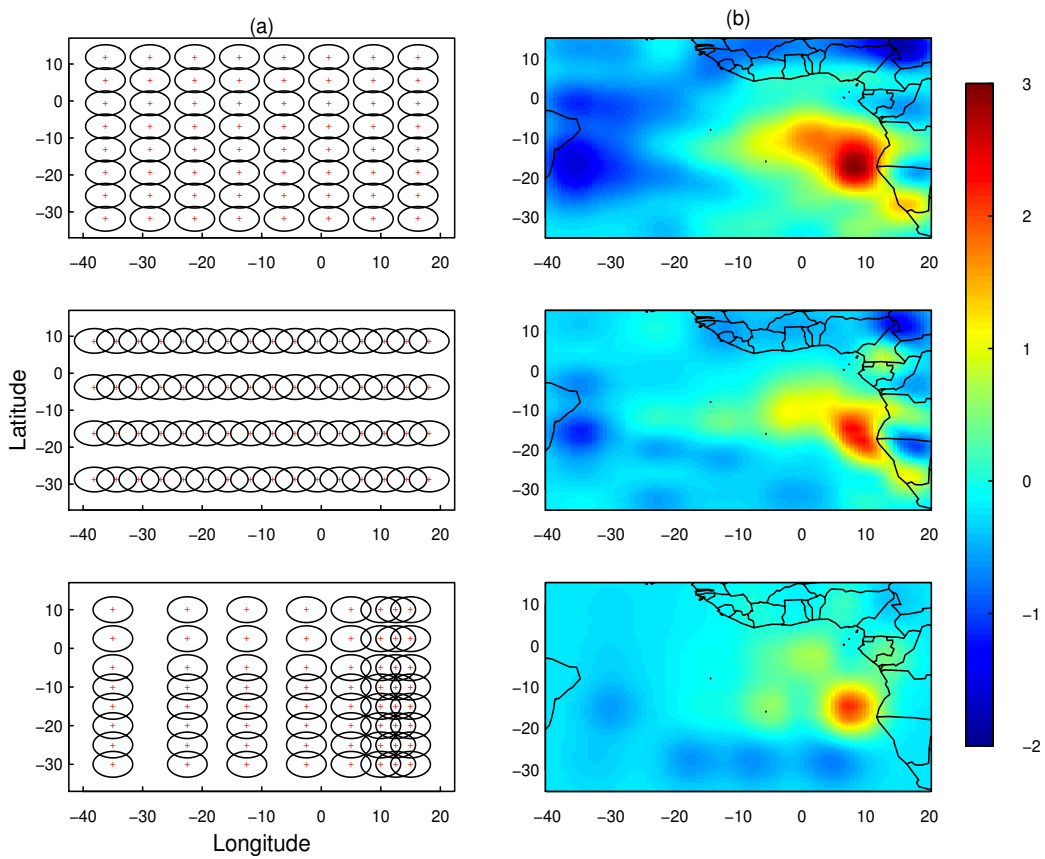


Fig. 7 Comparison of the posterior mean of the overall bias $\mu(s)$ for three different choices of kernel locations: (a) Gaussian weighting kernel locations; (b) the posterior mean surfaces of the overall common bias.

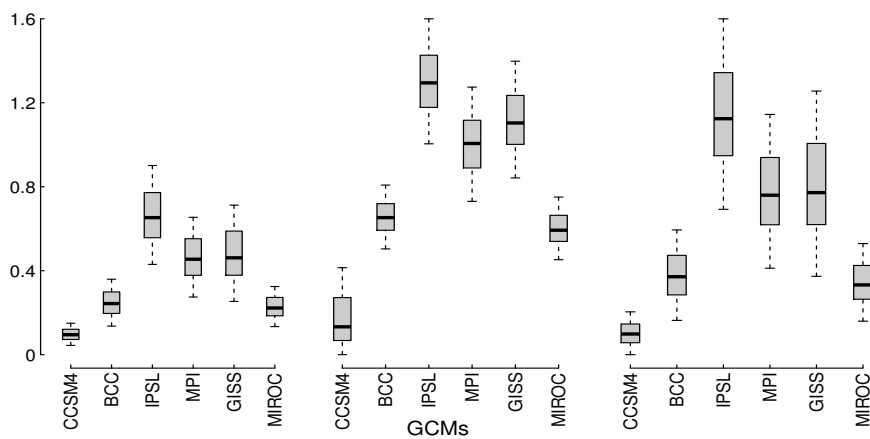


Fig. 8 Boxplots of MCMC draws associated to τ_j for different choices of the hyperparameter θ for the Half-Cauchy prior. Panels are for $\theta \in \{20, 35, 40\}$, respectively, from left to right.

The basic idea underlying our statistical model is generic and could be applied to a wider range of climate models, geographical locations and geophysical variables. Indeed this will be included in our future work that considers an extension to a spatiotemporal model involving a larger set of GCM simulations. The challenge will be to formulate a computationally efficient method for such an extensive approach taking into account the spatial and temporal features simultaneously. Another future focus is to consider biases of multivariate outputs from GCMs such as temperature and precipitation which may provide a broader assessments of climate model uncertainties.

Finally, in section 2.1 we have mentioned that we interpolated the outputs from the six GCMs to the same observational grid to resolve the misalignment between observations and model outputs before fitting the Bayesian hierarchical model. The uncertainty associated to the interpolation can affect the bias estimation in case of strong spatial misalignment. In our case study, both reanalysis and climate model outputs feature high spatial resolution over the investigated domain. We therefore expected interpolation to only minimally influence the results, and hence did not explicitly accounted for it in our model. Nonetheless, when there is concern of substantial uncertainty due to interpolation, it may be desirable to build a model that is able to handle such spatial misalignment directly. One possible approach is the Bayesian hierarchical method for nested block-level realignment (e.g., Banerjee et al. 2014), but this method requires the model output to be nested in the observational grid (Mugglin and Carlin 1998). A simpler solution is, once the outputs are firstly predicted to the observational grid using a stochastic model based approach such as the kriging method, to rectify the uncertainty that has been introduced by inflating the variance of the error $\varepsilon_j(s)$ in model (2). We denote the predicted value from climate model j at spatial location s by $\hat{X}_j(s)$. Its variance, $\delta_j^2(s) = \text{var}(\hat{X}_j(s))$ is zero if the output grid and observation grid coincide in s , otherwise it will be positive. Thus we specify

$$\text{var}(\varepsilon_j(s)) = \sigma_j^2 + \gamma_j \delta_j^2(s),$$

where the modulating parameter γ_j is positive. This slight modification adds further parameters to the Bayesian hierarchical model for which we can assign prior distributions similarly to σ_j^2 .

Acknowledgements The research leading to these results has received funding from the European Union, Seventh Framework Programme (FP7/2007-2013) under Grant agreement n 603521 - PREFACE. The authors would like to thank the two anonymous reviewers and the associate editor for helpful comments on the manuscript.

6 Appendix: choice of priors

In this section, we provide details of prior and hyperparameters choices. All priors are approximately non-informative. For the error variances $\{\sigma_{\varepsilon,j}^2 : j = 1 \dots, 6\}$, we assign the uniform prior on the standard deviation scale $\sigma_{\varepsilon,j} \sim \text{Unif}(a, b)$ by choosing $a = 0$ and $b = 10^2$ for each j independently. Accordingly, the error variances, which are proportional to $(b - a)^2$, are very large so that the priors are approximately non-informative. For $\{\tau_j^2 : j = 1 \dots, 6\}$, we use a Half-Cauchy (HC) prior, which is a conditionally conjugate family of a half t distribution (Gelman 2006). The Half t distribution corresponds to the absolute value of a Student-t distribution centered at zero, whose probability distribution is proportional to

$$\left(1 + \frac{1}{\text{df}} \left(\frac{\tau_j}{\theta}\right)^2\right)^{-(\text{df}+1)/2} \quad (8)$$

with two parameters: degrees of freedom df and scale parameter θ . We obtain the proper HC probability distribution for τ_j as a special case of (8) by setting $\text{df} = 1$,

$$p(\tau_j) \propto (\theta^2 + \tau_j^2)^{-1}, \quad j = 1, \dots, 6$$

we specify priors for τ_j as $\tau_j \sim \text{HC}(\theta)$, independently for each j . Large but finite value of the scale parameter θ represents an approximately non-informative prior distribution. In the limit $\theta \rightarrow \infty$ this becomes a uniform prior density on $p(\tau_j)$. For our analysis, we set $\theta = 30$. To choose a prior for the $p \times p$ covariance matrix \mathbf{G} , the variances G_1, \dots, G_p and the pair-wise covariances $G_{kl} : k, l = 1, \dots, p$ must be explicitly specified. One way to achieve this is to use the separation technique (Gelman and Hill 2006; O'Malley et al. 2008)

$$\mathbf{G} = \Gamma \mathbf{Q} \Gamma$$

where Γ is the diagonal matrix with diagonal elements $\omega_1^2, \dots, \omega_p^2$ and \mathbf{Q} is new $p \times p$ covariance matrix. The role of the new parameters ω_k^2 and \mathbf{Q} is to derive appropriately scaled priors for the variances and pair-wise covariances related to \mathbf{G} . We assign proper uniform prior on $\omega_k^2 \sim \text{Unif}(0, 10^2)$ independently for each k . The covariance component \mathbf{Q} is given the inverse Wishart distribution $\text{IW}(p+1, \mathbf{I}_p)$. The two parameters degrees of freedom $p+1$ and the identity matrix \mathbf{I}_p fully determine the distribution. The variances and pair-wise covariances associated to \mathbf{G} are then obtained as $G_k = \omega_k^2 Q_p$ and $G_{kl} = \omega_k \omega_l Q_{kl}$. To make inference, we require the standard deviations $|G_k|^{1/2}$ and correlations ρ_{kl}

$$|G_k|^{1/2} = |\omega_k| \sqrt{Q_k} \quad \text{and} \quad \rho_{kl} = \frac{G_{kl}}{|G_k|^{1/2} |G_l|^{1/2}}, \quad k, l = 1, \dots, p$$

References

- 635 **References**
- 636 Banerjee S, Carlin BP, Gelfand AE (2014) Hierarchical
637 modeling and analysis for spatial data. CRC Press, New
638 York
- 639 Berliner LM (2003) Physical-statistical modeling in geo-
640 physics. *Journal of Geophysical Research: Atmospheres*
641 108:8776. doi:10.1029/2002JD002865
- 642 Boberg F, Christensen JH (2012) Overestimation of
643 Mediterranean summer temperature projections due to
644 model deficiencies. *Nature Climate Change* 2:433-436
- 645 Brohan P, Kennedy JJ, Harris I, Tett SF, Jones PD
646 (2006) Uncertainty estimates in regional and global ob-
647 served temperature changes: A new data set from 1850.
648 *Journal of Geophysical Research: Atmospheres* 111.
649 doi:10.1029/2005JD006548
- 650 Buser CM, Knsch HR, Lthi D, Wild M, Schr C (2009)
651 Bayesian multi-model projection of climate: bias as-
652 sumptions and interannual variability. *Climate Dynamics*
653 33:849-868
- 654 Christensen JH, Boberg F, Christensen OB, LucasPicher
655 P (2008) On the need for bias correction of re-
656 gional climate change projections of temperature
657 and precipitation. *Geophysical Research Letters* 35.
658 doi:10.1029/2008GL035694
- 659 Cowles MK, Carlin BP (1996) Markov chain Monte Carlo
660 convergence diagnostics: a comparative review. *Journal of*
661 *the American Statistical Association* 91:883-904
- 662 Cressie N (1993) *Statistics for spatial data*. Wiley-
663 Interscience, New York
- 664 Flato, G., J. Marotzke, B. Abiodun, P. Braconnot, S.C. Chou,
665 W. Collins, P. Cox, F. Driouech, S. Emori, V. Eyring, C.
666 Forest, P. Gleckler, E. Guilyardi, C. Jakob, V. Kattsov,
667 C. Reason and M. Rummukainen, 2013: Evaluation of
668 Climate Models. In: *Climate Change 2013: The Physical*
669 *Science Basis*. Contribution of Working Group I to the
670 *Fifth Assessment Report of the Intergovernmental Panel*
671 *on Climate Change* [Stocker, T.F., D. Qin, G.-K. Plattner,
672 M. Tignor, S.K. Allen, J. Boschung, A. Nauels, Y. Xia,
673 V. Bex and P.M. Midgley (eds.)]. Cambridge University
674 Press, Cambridge, United Kingdom and New York, NY,
675 USA
- 676 Furrer R, Sain SR, Nychka D, Meehl GA (2007) Multi-
677 variate Bayesian analysis of atmosphereocean general cir-
678 culation models. *Environmental and Ecological Statistics*
679 14:249-266
- 680 Gelfand AE, Diggle P, Fuentes M, Guttorp P (2010) *Hand-*
681 *book of Spatial Statistics*. Chapman and Hall / CRC,
682 Florida
- 683 Gelman A (2006) Prior distributions for variance parameters
684 in hierarchical models (comment on article by Browne
685 and Draper). *Bayesian Analysis* 1:515-534
- Gelman A, Hill J (2006) *Data analysis using regression* 686
and multilevel/hierarchical models. Cambridge Univer- 687
sity Press, Cambridge 688
- Gilks WR, Richardson S, Spiegelhalter DJ (1996) *Markov* 689
chain Monte Carlo in practice. Chapman and Hall, Lon- 690
don 691
- Higdon D (1998) A process-convolution approach to mod- 692
elling temperatures in the North Atlantic Ocean. *Environ-* 693
mental and Ecological Statistics 5:173-190 694
- Jun M, Knutti R, Nychka DW (2008) Spatial analysis to 695
quantify numerical model bias and dependence: how 696
many climate models are there?. *Journal of the American* 697
Statistical Association 103:934-947 698
- Kalnay E, Kanamitsu M, Kistler R, Collins W, Deaven D, 699
Gandin L, Iredell M, Saha S, White G, Woollen J, Zhu 700
Y (1996) The NCEP/NCAR 40-year reanalysis project. 701
Bulletin of the American Meteorological Society 77:437- 702
471 703
- Kang EL, Cressie N, Sain SR (2012) Combining outputs 704
from the North American regional climate change assess- 705
ment program by using a Bayesian hierarchical model. 706
Journal of the Royal Statistical Society: Series C (Applied 707
Statistics) 61:291-313 708
- Kaufman CG, Sain SR (2010) Bayesian functional ANOVA 709
modeling using Gaussian process prior distributions, 710
Bayesian Analysis 5:123-149 711
- Keller CF (2009) Global warming: a review of this mostly 712
settled issue. *Stochastic Environmental Research and* 713
Risk Assessment 23:643676 714
- Kistler R, Collins W, Saha S, White G, Woollen J, Kalnay E, 715
Chelliah M, Ebisuzaki W, Kanamitsu M, Kousky V, van 716
den Dool H (2001) The NCEP-NCAR 50-year reanalysis: 717
Monthly means CD-ROM and documentation. *Bulletin of* 718
the American Meteorological society 82:247-267 719
- Knutti R (2010) The end of model democracy? An editorial 720
comment. *Climatic Change* 102:395404 721
- Lambert SJ, Boer GJ (2001) CMIP1 evaluation and inter- 722
comparison of coupled climate models. *Climate Dynam-* 723
ics 17:83-106 724
- Leith NA, Chandler RE (2010) A framework for interpret- 725
ing climate model outputs. *Journal of the Royal Statistical* 726
Society: Series C (Applied Statistics) 59:279-296 727
- Milinski, S., J. Bader, H. Haak, A. C. Siongo, J. H. 728
Jungclaus (2016) High atmospheric horizontal resolution 729
eliminates the wind-driven coastal warm bias in the south- 730
eastern tropical Atlantic. *Geophysical Research Letter*, 731
accepted for publication 732
- Mugglin AS, Carlin BP (1998) Hierarchical modeling in Ge- 733
ographic Information Systems: population interpolation 734
over incompatible zones. *Journal of Agricultural, Biologi-* 735
cal and Environmental Statistics 3: 111130 736
- Neuman SP (2003) Maximum likelihood Bayesian averag- 737
ing of uncertain model predictions. *Stochastic Environ-* 738

- 739 mental Research and Risk Assessment 17: 291-305
- 740 O'Malley AJ, Zaslavsky AM (2008) Domain-level covari-
741 ance analysis for multilevel survey data with structured
742 nonresponse. *Journal of the American Statistical Associ-*
743 *ation* 103:1405-1418
- 744 Polson NG, Scott JG (2012) On the half-Cauchy prior for a
745 global scale parameter. *Bayesian Analysis* 7:887-902
- 746 Sain SR, Furrer R (2010) Combining climate model out-
747 put via model correlations. *Stochastic Environmental Re-*
748 *search and Risk Assessment* 24:821-829
- 749 Stroud JR, Miller P, Sansó B (2001) Dynamic models for
750 spatiotemporal data. *Journal of the Royal Statistical Soci-*
751 *ety. Series B, Statistical Methodology* 63: 673-689
- 752 Taylor KE, Stouffer RJ, Meehl GA (2012) An overview of
753 CMIP5 and the experiment design. *Bulletin of the Amer-*
754 *ican Meteorological Society* 93:485-498
- 755 Tebaldi C, Smith RL, Nychka D, Mearns LO (2005) Quan-
756 tifying uncertainty in projections of regional climate
757 change: A Bayesian approach to the analysis of multi-
758 model ensembles. *Journal of Climate* 18:1524-1540
- 759 Toniazzo T, Woolnough S (2014) Development of warm
760 SST errors in the southern tropical Atlantic in CMIP5
761 decadal hindcasts. *Climate Dynamics* 43:2889-2913
- 762 Wahl, S., M. Latif, W. Park, N. Keenlyside (2015) On
763 the Tropical Atlantic SST warm bias in the Kiel Cli-
764 mate Model. *Climate Dynamics* doi:10.1007/s00382-
765 009-0690-9
- 766 Wang C, Zhang L, Lee SK, Wu L, Mechoso CR (2014) A
767 global perspective on CMIP5 climate model biases. *Nat-*
768 *ure Climate Change* 4: 201-205
- 769 Zanchettin D, Bothe O, Lehner F, Ortega P, Raible CC,
770 Swingedouw D (2015) Reconciling reconstructed and
771 simulated features of the winter Pacific/North American
772 pattern in the early 19th century. *Climate of the Past*
773 11:939-958